Sign Change of Spin-Orbit Torque in Pt/NiO/CoFeB Structures

Zhu, Dapeng; Zhang, Tianrui; Fu, Xiao; Hao, Runrun; Hamzić, Amir; Yang, Huaiwen; Zhang, Xueying; Zhang, Hui; Du, Ao; Xiong, Danrong; ...

Source / Izvornik: **Physical Review Letters, 2022, 128**

Journal article, Published version
Rad u časopisu, Objavljena verzija rada (izdavačev PDF)

https://doi.org/10.1103/PhysRevLett.128.217702

Permanent link / Trajna poveznica: https://urn.nsk.hr/urn:nbn:hr:217:512543

Editors' Suggestion

Sign Change of Spin-Orbit Torque in Pt/NiO/CoFeB Structures

Dapeng Zhu,[1,2] Tianrui Zhang,[1] Xiao Fu,[1,2] Runrun Hao,[1,2] Amir Hamzić,[1,3] Huaiwen Yang,[1,2] Xueying Zhang,[1,2] Hui Zhang,[1] Ao Du,[1] Danrong Xiong,[1] Kewen Shi,[1] Shishen Yan,[4] Shufeng Zhang,[5] Albert Fert,[1,6] and Weisheng Zhao[1,2,*]

[1]*Fert Beijing Institute, MIIT Key Laboratory of Spintronics, School of Integrated Circuit Science and Engineering, Beihang University, Beijing 100191, China*

[2]*Beihang-Goertek Joint Microelectronics Institute, Qingdao Research Institute, Beihang University, Qingdao 266000, China*

[3]*Department of Physics, Faculty of Science, University of Zagreb, Zagreb HR-10001, Croatia*

[4]*School of Physics, State Key Laboratory of Crystal Materials, Shandong University, Jinan 250100, China*

[5]*Department of Physics, University of Arizona, Tucson, Arizona 85721, USA*

[6]*Unité Mixte de Physique, CNRS, Thales, Université Paris-Saclay, Palaiseau 91767, France*

(Received 17 February 2021; revised 30 January 2022; accepted 20 April 2022; published 25 May 2022)

Antiferromagnetic insulators have recently been proved to support spin current efficiently. Here, we report the dampinglike spin-orbit torque (SOT) in Pt/NiO/CoFeB has a strong temperature dependence and reverses the sign below certain temperatures, which is different from the slight variation with temperature in the Pt/CoFeB bilayer. The negative dampinglike SOT at low temperatures is proposed to be mediated by the magnetic interactions that tie with the "exchange bias" in Pt/NiO/CoFeB, in contrast to the thermal-magnon-mediated scenario at high temperatures. Our results highlight the promise to control the SOT through tuning the magnetic structure in multilayers.

DOI: 10.1103/PhysRevLett.128.217702

Antiferromagnets (AFM) have gained considerable interest in the field of spintronics due to their unique properties such as robustness against external magnetic disturbance, absence of stray field, and spin dynamics in the terahertz range [1–3]. In particular, the AFM insulators have been proved to support spin current with high efficiency [4–9] and long distance [4,10–12], through different experiments such as the spin Seebeck effect [6–9], spin pumping [4,5], spin-torque ferromagnetic resonance [13], and nonlocal spin transport [10–12]. Motivated to minimize the Joule heat dissipation associated with the electron motion, magnon mediated spin-orbit torque (SOT) and magnetization switching have been further demonstrated through inserting an AFM insulator between the heavy metal (HM) and ferromagnet (FM) layers [14–16], which highlights the great promise of the AFM insulators for exploring energy-efficient SOT-based spintronics.

Toward understanding the spin transmission processes in magnetic multilayers with an AFM insulator, intensive studies have demonstrated that the coherent propagation of evanescent spin waves [17,18], diffusion of incoherent magnons [19], and thermal-gradient-driven magnon current in the AFM insulator [11] play important roles in mediating the spin current at high temperatures. These previous works mainly focused on the spin dynamics of magnetic moments inside the AFM insulator. However, the multiple interfaces in magnetic multilayer structures may also have significant impacts. A few recent studies have revealed the HM/AFM interface affects the spin reflection processes greatly at low temperatures, which gives rise to a negative spin Hall magnetoresistance (SMR) effect [20,21]. The HM/FM interface has also been reported to strongly affect the spin transmission and spin relaxation across the interface [22,23]. On the other side, the AFM/FM interface is well known to hold interfacial exchange coupling, which brings about the effects such as coercivity enhancement and "exchange bias" [24]. Nevertheless, the role of magnetic interactions at the AFM/FM interface has yet to be investigated in the framework of mediating spin-orbit torque.

In this Letter, with the insertion of a prototypical AFM insulator NiO between Pt and CoFeB, we report the dampinglike SOT strongly depends on the temperature and reverses the sign below certain temperatures, in contrast to the weak temperature dependence of that in Pt/CoFeB bilayer. The negative dampinglike SOT at low temperatures cannot be captured by the common mediation schemes via magnons and spin waves, but be mediated by the magnetic interactions in the heterostructure. The SMR ratio was found to reverse sign as well at low temperatures in Pt/NiO/CoFeB, with the sign-change temperature higher than that of the dampinglike SOT. Both the negative SOT and SMR at low temperatures can be understood within a "spin-flop" picture between the magnetic moments of NiO and CoFeB. These results highlight the significance of magnetic interactions in mediating SOT in multilayers, which will promote the AFM insulator-based SOT applications.

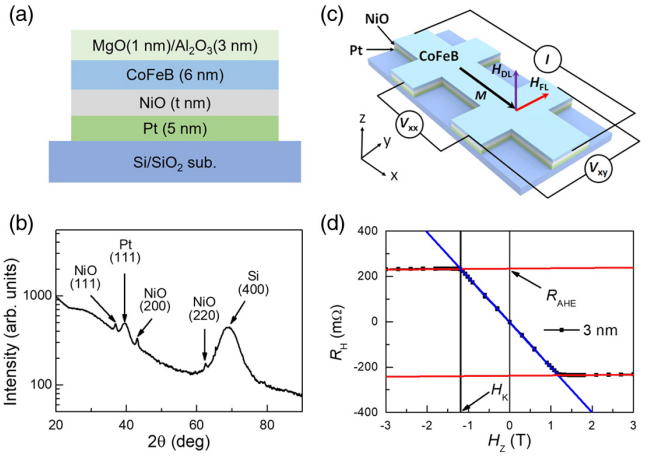

FIG. 1. (a) The stack layer structure of the samples, with a $\mathrm{MgO}(1)/\mathrm{Al_2O_3}(3)$ capping layer to protect the underneath layers from degradation. (b) The x-ray diffraction patterns for the sample with NiO of 50 nm. (c) The schematic of measurement configuration for the electrical transport experiments. (d) The perpendicular magnetic field (H_z) dependence of the Hall resistance (R_H) for the sample with 3 nm NiO at 300 K.

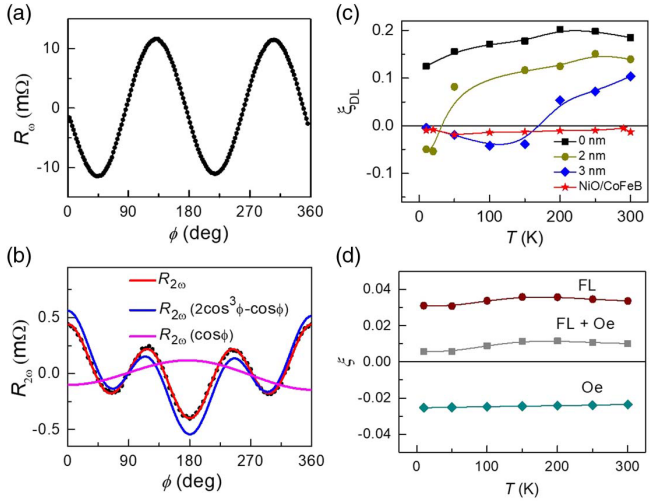

FIG. 2. (a),(b) The first (R_ω) and the second ($R_{2\omega}$) harmonic Hall resistance as a function of in-plane rotation angle ϕ for the sample with 3 nm NiO at 300 K, under external magnetic field of 30 mT. The decomposed $\cos\phi$ and $2\cos^3\phi - \cos\phi$ terms of the $R_{2\omega}$ are also displayed in (b). (c) The obtained ξ_{DL} for the samples with NiO of 0, 2, and 3 nm, and the NiO/CoFeB sample at different temperatures. (d) The ξ of $H_{\mathrm{FL}} + H_{\mathrm{Oe}}$ (FL + Oe), H_{Oe} (Oe), and H_{FL} (FL) for the sample with 3 nm NiO at different temperatures.

Thin film stacks of $\mathrm{Pt}(5)/\mathrm{NiO}(t)/\mathrm{CoFeB}(6)/\mathrm{MgO}(1)/\mathrm{Al_2O_3}(3)$ were deposited on thermally oxidized Si substrates by using magnetron sputtering with base pressure less than 2×10^{-9} Torr, where the thicknesses in parentheses are in nanometers and $t = 0$, 2, 3, and 50. As schematically shown in Fig. 1(a), the capping layer of $\mathrm{MgO}(1)/\mathrm{Al_2O_3}(3)$ works as a protection for the underneath layers from degradation. X-ray diffraction patterns of the sample with 50 nm NiO are plotted in Fig. 1(b), which shows the Pt, NiO, and CoFeB have the (111)-preferred orientation, polycrystalline, and amorphous structure, respectively. For the transport measurements, Hall bar devices with a channel length of 20 μm and a channel width of 5 μm were fabricated using standard photolithography and Ar ion milling. The harmonic Hall method considering the anomalous Hall effect (AHE) and planar Hall effect (PHE) was used to investigate the SOT, which allows us to quantify the SOT free from thermal effects [25–27]. Figure 1(c) shows the schematic configuration of the electrical transport experiments.

The AHE was first measured, and the perpendicular magnetic field (H_z) dependence of the Hall resistance (R_H) is shown in Fig. 1(d), for the sample with 3 nm NiO at 300 K. From the R_H-H_z curve, both the anomalous Hall resistance R_{AHE} and effective perpendicular magnetic anisotropy field H_K can be obtained by fitting linear functions to the low-field and high-field regions. The R_{AHE} has a monotonic decrease with decreasing the temperature (see Supplemental Material [28]). For the harmonic Hall measurements, ac currents with a frequency of 133.33 Hz were applied through the Hall bar devices while rotating the external magnetic field (H_{ext}) of constant magnitude in the xy plane. The first (V_ω) and second ($V_{2\omega}$) harmonic Hall voltages were recorded by two lock-in amplifiers. Figures 2(a) and 2(b) show the first (R_ω) and second ($R_{2\omega}$) harmonic Hall resistance respectively as a function of the in-plane rotation angle ϕ, for the sample with 3 nm NiO at 300 K and H_{ext} of 30 mT. As can be observed, the R_ω follows the $\sin 2\phi$ dependence, which indicates the moment of CoFeB follows the external magnetic field. The planar Hall resistance R_{PHE} can be extracted from fitting the R_ω-ϕ curve to $R_\omega = R_{\mathrm{PHE}} \sin 2\phi$. The R_{PHE} also shows a monotonic decrease with decreasing the temperature (see Supplemental Material [28]).

The SOT is known to consist of two components: dampinglike toque $\boldsymbol{\tau}_{\mathrm{DL}} \sim \mathbf{m} \times (\mathbf{m} \times \boldsymbol{\sigma})$ and fieldlike torque $\boldsymbol{\tau}_{\mathrm{FL}} \sim \mathbf{m} \times \boldsymbol{\sigma}$, where $\mathbf{m}$ and $\boldsymbol{\sigma}$ are the magnetization unit vector and spin accumulation vector, respectively [41,42]. The oscillating SOT induced by the ac current drive the CoFeB magnetization to oscillate both in-plane and out-of-plane, resulting in the $R_{2\omega}$ following $R_{2\omega} = -\{R_{\mathrm{AHE}}[H_{\mathrm{DL}}/(H_{\mathrm{ext}} - H_K)] + R_T\}\cos\phi + 2R_{\mathrm{PHE}}[(H_{\mathrm{FL}} + H_{\mathrm{Oe}})/H_{\mathrm{ext}}] \times (2\cos^3\phi - \cos\phi)$ [25–27], where H_{DL} and H_{FL} denote the dampinglike and fieldlike spin-orbit effective fields respectively, H_{Oe} is the Oersted field induced by current, and R_T is the second harmonic Hall resistance owing to thermal effects. From the $\cos\phi$ term of $R_{2\omega}$ obtained at different H_{ext} that is sufficiently high to saturate the CoFeB magnetization, the H_{DL} and R_T can be determined (see Supplemental Material [28]). A dimensionless dampinglike SOT efficiency ξ_{DL} can be further calculated by $\xi_{\mathrm{DL}} = (2eH_{\mathrm{DL}}m_s/\hbar J)$ [43], where m_s is the spontaneous

magnetic moment per unit area, J is the current density through Pt, e is the electron charge, and $\hbar = h/(2\pi)$ is the reduced Planck constant.

Figure 2(c) summarizes the ξ_{DL} for the Pt/NiO/CoFeB samples with NiO of 0, 2, and 3 nm, and the NiO/CoFeB sample at different temperatures. As a result, the ξ_{DL} for the Pt/CoFeB slightly decreases from ~0.18 at 300 K to ~0.12 with decreasing the temperature to 10 K, which is consistent with the previous reports for the spin Hall angle of Pt [26,44–46]. After inserting 2 (3) nm NiO between the Pt and CoFeB, the ξ_{DL} reduces to ~0.14 (0.1) at 300 K, indicating the spin current transmitting through the NiO layer. More importantly, different from the weak temperature dependence in the Pt/CoFeB bilayer, the ξ_{DL} in the Pt/NiO/CoFeB trilayer shows a strong temperature dependence and reverses the sign at around 30 (170) K for the sample with 2 (3) nm NiO. For the NiO/CoFeB bilayer, the ξ_{DL} shows negative values and weak temperature dependence, with the absolute values much smaller than that of the Pt/CoFeB and Pt/NiO/CoFeB samples. The extracted R_T is found to change with varying the temperature, probably due to the different temperature gradients and/or associated with the NiO.

From the $2\cos^3\phi - \cos\phi$ term of $R_{2\omega}$ at different H_{ext}, the $H_{FL} + H_{Oe}$ can be determined (see Supplemental Material [28]). After subtracting the H_{Oe} calculated by the Ampère's law [27,47], the H_{FL} was further obtained. The effective efficiency ξ for $H_{FL} + H_{Oe}$, H_{Oe}, and H_{FL} calculated by $\xi = (2eHm_s/\hbar J)$ were shown in Fig. 2(d) for the sample with 3 nm NiO. As can be observed, the ξ of H_{FL} does not change much with varying temperature, which is different from the ξ_{DL}. Similar results were also found in the H_{FL} for the sample with 2 nm NiO (see Supplemental Material [28]). The fieldlike SOTs in multilayers have been widely considered to arise mainly from the Rashba effect at interface with broken inversion symmetry [48,49]. While recent studies suggest the Rashba effect giving rise to a dampinglike SOT as well [50,51], this dampinglike SOT should take a same temperature dependence with the fieldlike counterpart as both of them are linearly proportional to the Rashba parameter α_R [52]. The abnormal dampinglike SOT observed at low temperatures in the Pt/NiO/CoFeB may have an origin different from the fieldlike SOT counterpart, with the latter one being probably related with the Rashba effect at the Pt/NiO interface (see Supplemental Material [28]).

In order to gain a comprehensive understanding of the spin transmission processes in the Pt/NiO/CoFeB, SMR experiments were further conducted. A charge current (J_C) was applied parallel to the x axis, and the longitudinal resistance was recorded with rotating a magnetic field ($\mathbf{H}$) of 3 T in the yz plane. Depending on the $\mathbf{H}$ direction, the spin accumulation at the Pt/NiO interface and thus the inverse spin Hall current J_C^{ISHE} in Pt will change, leading to the conductivity of Pt being modified. We define the sample resistance as $R_{||}$ ($R_\perp$) with the $\mathbf{H}$ parallel (perpendicular) to the y axis, and the SMR ratio equal to $(R_\perp - R_{||})/R_0$, where R_0 is the sample resistance at zero magnetic field. Figure 3(a) shows the obtained SMR ratio for Pt/NiO/CoFeB samples with NiO of 0, 2, and 3 nm at different temperatures. For the Pt/CoFeB bilayer, the SMR ratio is positive and has a weak temperature dependence. The positive SMR ratio means the $R_\perp > R_{||}$, i.e., the J_C^{ISHE} maximizes when $\mathbf{H}\|\boldsymbol{\sigma}$ and minimizes when $\mathbf{H}\perp\boldsymbol{\sigma}$, which is consistent with the previous reports [53]. For the samples with NiO layer, the SMR ratio reduces as compared with that of Pt/CoFeB at 300 K, and it shows a strong temperature dependence and reverses the sign below 150 K (250 K) for the sample with NiO of 2 (3) nm. The negative SMR ratio means $R_\perp < R_{||}$, i.e., the J_C^{ISHE} maximizes when $\mathbf{H}\perp\boldsymbol{\sigma}$ and minimizes when $\mathbf{H}\|\boldsymbol{\sigma}$.

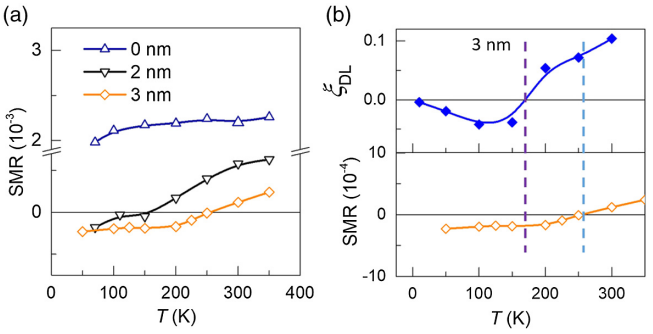

FIG. 3. (a) The obtained SMR ratio for the samples with NiO of 0, 2, and 3 nm at different temperatures. (b) Comparison of the temperature dependence of the dampinglike SOT efficiency and the SMR ratio for the sample with 3 nm NiO.

Now we discuss the temperature dependence of the ξ_{DL} and SMR in the Pt/NiO/CoFeB structure. At high temperatures, the spin current transfer from Pt to CoFeB via NiO layer is well understood. Spin excitations of the NiO layer are abundant at high temperatures, either in the form of magnons or of short-ranged spin fluctuations, which carry intrinsic angular moments. When the electron spin current created by Pt enters the NiO layer, the nonequilibrium magnons are generated at the Pt/NiO interface and subsequently diffuse to the other side of the interface NiO/CoFeB, leading to a spin torque on CoFeB or being reflected to Pt. In this process, the NiO serves as a spin-current medium, and the SMR ratio and the dampinglike SOT have a normal sign. A number of experiments have already demonstrated that the NiO is capable of propagating the spin current that originated from the spin pumping [4,54] and the thermal gradient [9], similar to the present experiment.

To understand the negative sign of the ξ_{DL} at low temperatures, we first consider the spin transport processes through the NiO layer. Bulk NiO is known as a biaxial AFM insulator with two highly elliptical magnon eigenmodes with eigenfrequencies of 0.14 and 1.07 THz [55]. Theoretical studies suggest that the coherent propagation of

the above evanescent spin waves [17,18] and the diffusion of the incoherent magnons generated by the magnon accumulation at interfaces [19], may provide an explanation for the observed enhancement of spin current transmission in NiO at high temperatures [18,19]. However, these mechanisms predict a monotonical increase of the spin current transmission with the increase of temperature (up to the Néel temperature of NiO), and thus they are unable to explain the sign reverse of the dampinglike SOT at a certain temperature. Another plausible source for the spin transmission in the AFM insulator has been attributed to the spin Seebeck effect in which the thermal gradient drives a thermal magnon current across the NiO layer [11]. Similarly, this picture does not work for the low temperature where the magnon population is significantly reduced and thus the spin current flowing from Pt to CoFeB is negligible. Would it be possible that the observed negative sign of the SOT at low temperatures comes from the interface of NiO/CoFeB alone? As shown in Fig. 2(c), although the sign is indeed negative, the absolute value of the ξ_{DL} in NiO/CoFeB is too small to be responsible for the observed negative ξ_{DL} in the Pt/NiO/CoFeB samples. Therefore, the spin torque received by CoFeB originates from the spin Hall current of the Pt layer. We propose below that the magnetic coupling within the NiO layer and at the interface could be responsible for mediating the spin torque at low temperatures.

The magnetic configuration at the interface between a magnetic layer CoFeB and the antiferromagnetic layer NiO is generally complex, in which the "exchange bias" phenomenon displays complicated magnetic properties. Here, we shall start by considering a simple "spin-flop" model proposed by Koon [56], which was initially developed to explain the "exchange bias" effect in thin films with compensated FM/AFM interfaces. In this model, the ground state configuration corresponds to perpendicular orientation of the bulk FM moments with respect to the AFM magnetic easy axis direction, and the magnetic moments of the sublattice in AFM interfacial layer exhibit canted magnetic moments with a small canting angle relative to the AFM bulk easy axis as schematically shown in Fig. 4(b). The above "spin-flop" configuration of magnetic moments at FM/AFM interfaces has previously been experimentally confirmed by techniques such as x-ray magnetic linear dichroism and photoemission electron-beam microscopy [57,58]. This assumed magnetic configuration has already been used for explaining the negative SMR ratio at low temperatures observed in the YIG/NiO/Pt structure [54]. The negative SMR ratio in the Pt/NiO/CoFeB at low temperatures probably has a same origin since the interfacial spin orbit coupling at the NiO/CoFeB interface should be weak as suggested by the negligible ξ_{DL} in Fig. 2(c).

Now let us turn on a simple form of magnetic coupling at two interfaces, as schematically shown in Figs. 4(c) and 4(e), $E = -A\mathbf{m}_1 \cdot \mathbf{m}_2$, where $\mathbf{m}_1$ and $\mathbf{m}_2$ are the net moments at the interfaces of Pt/NiO and NiO/CoFeB.

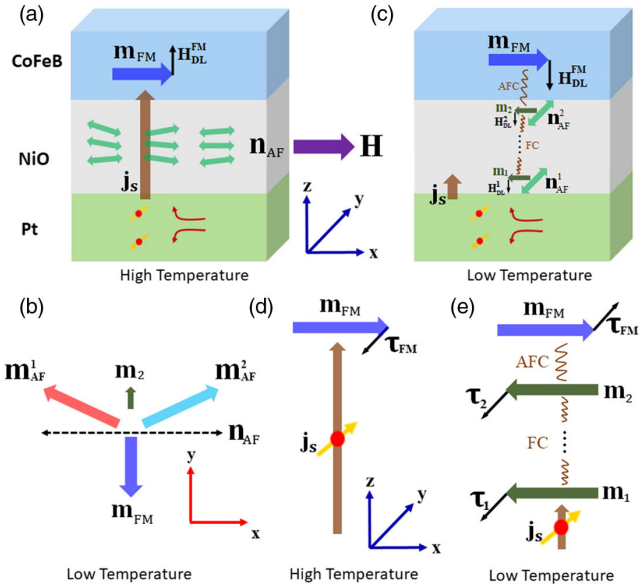

FIG. 4. (a) The schematic of the dampinglike spin-orbit effective fields (H_{DL}^{FM}) for the Pt/NiO/CoFeB at high temperature. (b) The schematic "spin-flop" configuration between the magnetic moments of the CoFeB ($\mathbf{m}_{FM}$) and NiO ($\mathbf{m}_{AF}^1$, $\mathbf{m}_{AF}^2$) at the NiO/CoFeB interface at low temperature. (c) The schematic of the dampinglike spin-orbit effective field for the Pt/NiO/CoFeB at low temperature. (d),(e) The schematic dampinglike SOTs for the Pt/NiO/CoFeB at high and low temperatures, respectively.

We further assume that $\mathbf{m}_1$ receives a torque from the spin Hall current of Pt and $\mathbf{m}_1$ is only coupled to $\mathbf{m}_2$, then we have $(d\mathbf{m}_1/dt) = \mathbf{j}_s - A\mathbf{m}_1 \times \mathbf{m}_2$, where $\mathbf{j}_s$ is the spin current absorbed by $\mathbf{m}_1$. In the steady state, we have $\mathbf{j}_s - A\mathbf{m}_1 \times \mathbf{m}_2 = 0$. On the other hand, the $\mathbf{m}_2$ is coupled with CoFeB through the "exchange bias" and one may assume that $\mathbf{m}_2$ is locked with the magnetization of CoFeB, and thus the spin torque on $\mathbf{m}_2$ received from $\mathbf{m}_1$ is, $-A\mathbf{m}_2 \times \mathbf{m}_1 = \mathbf{j}_s$. Therefore, the magnetic coupling between two magnetic moments at two sides of NiO interfaces can transfer the spin torque on the CoFeB without evolving the actual spin current flowing in the NiO layer. If the coupling between $\mathbf{m}_2$ and CoFeB is antiparallel, the dampinglike torque on CoFeB reverses sign compared to that at the high temperatures. A positive exchange bias field can be observed after cooling the sample with a large positive magnetic field and the sign of dampinglike SOT can be tuned by the positive exchange bias field at low temperatures, in consistence with the proposed scenario (see Supplemental Material [28]).

The above model ties the low-temperature spin torque with the "exchange bias." In the "exchange bias," the rotation of $\mathbf{m}_2$ leads to the change of the $\mathbf{m}_1$, while in the spin torque, the direction of $\mathbf{m}_1$ affects $\mathbf{m}_2$. When the temperature is above the blocking temperature of the NiO, the magnetic moments in NiO are significantly reduced and the transfer of the torque through exchange coupling in NiO disappears as well. Comparing the

temperature dependences of the ξ_{DL} and SMR ratio as shown in Fig. 3(b), we find that the sign-change temperature of the ξ_{DL} is lower than that of the SMR ratio. This result may be attributed to the different schemes between the SMR and the dampinglike spin torque: the negative SMR at low temperatures involves the reflected spin current primarily given by the presence of Néel vector, which is related with the characteristic temperature of Néel temperature; the negative dampinglike spin torque at low temperatures relies on the spin torque transfer via the spin-flop canting of the NiO moments, which is related with the blocking temperature of the NiO/CoFeB. Since the blocking temperature is commonly lower than the Néel temperature, it is reasonable that the sign-change temperature is lower for the ξ_{DL} than the SMR. In addition, we note that the magnetic proximity effect may also emerge at the Pt/NiO interface at low temperatures [59], and it is unclear what is the role of this proximity played in the sign-change.

In conclusion, we have observed that the dampinglike SOT in the Pt/NiO/CoFeB structures reverses the sign below certain temperatures with the sign-change temperature lower than that of the SMR ratio. The negative dampinglike SOT and SMR results at low temperatures can be understood under the "spin-flop" picture with an antiferromagnetic coupling between the net moment of NiO and CoFeB at the NiO/CoFeB interface. Here, the noncollinear magnetic configuration of NiO along with the magnetic interactions inside NiO and at NiO/CoFeB interface are key ingredients for mediating the SOT at low temperatures. Plenty of AFM materials including metals and oxides and their heterostructures with ferromagnets may hold similar magnetic configuration and interactions at the interface [60,61], which can serve as an alternative platform toward noncollinear antiferromagnetic spintronics other than the materials with bulk noncollinear spin structures [62,63]. Our work demonstrates a new way to mediate and control the SOT without involving the moving charges, which will benefit for exploring the energy efficient spintronic devices.

This work was supported by National Key R&D Program of China (2021YFB3601303 and 2018YFB0407602), National Natural Science Foundation of China (Grant No. 11904017), the International Collaboration 111 Project (No. B16001), Beijing Municipal Science and Technology Project under Grant No. Z201100004220002, the Fundamental Research Funds for the Central Universities of China, and the Beijing Advanced Innovation Center for Big Data and Brain Computing (BDBC).

Note added.—Recently, Ref. [39] suggests the sign change of dampinglike SOT in Pt/NiO/CoFeB as being likely associated with the antiferromagnetic ordering or paramagnetic-antiferromagnetic transition in the NiO layer.

*weisheng.zhao@buaa.edu.cn

[1] V. Baltz, A. Manchon, M. Tsoi, T. Moriyama, T. Ono, and Y. Tserkovnyak, Rev. Mod. Phys. **90**, 015005 (2018).
[2] T. Jungwirth, X. Marti, P. Wadley, and J. Wunderlich, Nat. Nanotechnol. **11**, 231 (2016).
[3] P. Wadley *et al.*, Science **351**, 587 (2016).
[4] H. Wang, C. Du, P. C. Hammel, and F. Yang, Phys. Rev. Lett. **113**, 097202 (2014).
[5] C. Hahn, G. de Loubens, V. V. Naletov, J. Ben Youssef, O. Klein, and M. Viret, Europhys. Lett. **108**, 57005 (2014).
[6] S. Seki, T. Ideue, M. Kubota, Y. Kozuka, R. Takagi, M. Nakamura, Y. Kaneko, M. Kawasaki, and Y. Tokura, Phys. Rev. Lett. **115**, 266601 (2015).
[7] S. M. Wu, W. Zhang, A. KC, P. Borisov, J. E. Pearson, J. S. Jiang, D. Lederman, A. Hoffmann, and A. Bhattacharya, Phys. Rev. Lett. **116**, 097204 (2016).
[8] Z. Qiu, D. Hou, J. Barker, K. Yamamoto, O. Gomonay, and E. Saitoh, Nat. Mater. **17**, 577 (2018).
[9] W. Lin, K. Chen, S. Zhang, and C. L. Chien, Phys. Rev. Lett. **116**, 186601 (2016).
[10] W. Yuan *et al.*, Sci. Adv. **4**, eaat1098 (2018).
[11] R. Lebrun, A. Ross, S. A. Bender, A. Qaiumzadeh, L. Baldrati, J. Cramer, A. Brataas, R. A. Duine, and M. Kläui, Nature (London) **561**, 222 (2018).
[12] J. Han, P. Zhang, Z. Bi, Y. Fan, T. S. Safi, J. Xiang, J. Finley, L. Fu, R. Cheng, and L. Liu, Nat. Nanotechnol. **15**, 563 (2020).
[13] T. Moriyama, S. Takei, M. Nagata, Y. Yoshimura, N. Matsuzaki, T. Terashima, Y. Tserkovnyak, and T. Ono, Appl. Phys. Lett. **106**, 162406 (2015).
[14] H. Wang, J. Finley, P. Zhang, J. Han, J. T. Hou, and L. Liu, Phys. Rev. Applied **11**, 044070 (2019).
[15] Y. Wang *et al.*, Science **366**, 1125 (2019).
[16] K. Hasegawa, Y. Hibino, M. Suzuki, T. Koyama, and D. Chiba, Phys. Rev. B **98**, 020405(R) (2018).
[17] M. Dabrowski *et al.*, Phys. Rev. Lett. **124**, 217201 (2020).
[18] R. Khymyn, I. Lisenkov, V. S. Tiberkevich, A. N. Slavin, and B. A. Ivanov, Phys. Rev. B **93**, 224421 (2016).
[19] S. M. Rezende, R. L. Rodríguez-Suárez, and A. Azevedo, Phys. Rev. B **93**, 054412 (2016).
[20] G. R. Hoogeboom, A. Aqeel, T. Kuschel, T. T. M. Palstra, and B. J. van Wees, Appl. Phys. Lett. **111**, 052409 (2017).
[21] W. Lin and C. L. Chien, Phys. Rev. Lett. **118**, 067202 (2017).
[22] W. Zhang, W. Han, X. Jiang, S.-H. Yang, and S. S. P. Parkin, Nat. Phys. **11**, 496 (2015).
[23] J. C. Rojas-Sánchez, N. Reyren, P. Laczkowski, W. Savero, J.-P. Attané, C. Deranlot, M. Jamet, J.-M. George, L. Vila, and H. Jaffrès, Phys. Rev. Lett. **112**, 106602 (2014).
[24] J. Nogués and I. K. Schuller, J. Magn. Magn. Mater. **192**, 203 (1999).
[25] C. O. Avci, K. Garello, M. Gabureac, A. Ghosh, A. Fuhrer, S. F. Alvarado, and P. Gambardella, Phys. Rev. B **90**, 224427 (2014).
[26] Y.-C. Lau and M. Hayashi, Jpn. J. Appl. Phys. **56**, 0802B5 (2017).
[27] R. Itoh, Y. Takeuchi, S. DuttaGupta, S. Fukami, and H. Ohno, Appl. Phys. Lett. **115**, 242404 (2019).

[28] See Supplemental Material at http://link.aps.org/supplemental/10.1103/PhysRevLett.128.217702 for more information on the anomalous Hall effect at different temperatures, planar Hall effect at different magnetic fields and temperatures, second harmonic Hall measurements at different temperatures, exchange coupling between the NiO and CoFeB, influence of the spin torque transfer via Néel vector, second harmonic Hall signals in the x-z and y-z planes, different temperature dependence between the fieldlike and dampinglike torque, heating for the current flowing in the Pt and CoFeB layers, and influence of Rashba effect at the NiO/CoFeB interface, which includes Refs. [29–40].
[29] R. L. Stamps, J. Phys. D **33**, R247 (2000).
[30] S. DuttaGupta, A. Kurenkov, O. A. Tretiakov, G. Krishnaswamy, G. Sala, V. Krizakova, F. Maccherozzi, S. S. Dhesi, P. Gambardella, S. Fukami, and H. Ohno, Nat. Commun. **11**, 5715 (2020).
[31] J. Shi, V. Lopez-Dominguez, F. Garesci, C. Wang, H. Almasi, M. Grayson, G. Finocchio, and P. Khalili Amiri, Nat. Electron. **3**, 92 (2020).
[32] M. D. Stiles and R. D. McMichael, Phys. Rev. B **59**, 3722 (1999).
[33] S.-s. Yan, P. Grünberg, and R. Schäfer, Phys. Rev. B **62**, 5765 (2000).
[34] L. Baldrati *et al.*, Phys. Rev. Lett. **123**, 177201 (2019).
[35] X. Z. Chen, R. Zarzuela, J. Zhang, C. Song, X. F. Zhou, G. Y. Shi, F. Li, H. A. Zhou, W. J. Jiang, F. Pan, and Y. Tserkovnyak, Phys. Rev. Lett. **120**, 207204 (2018).
[36] R. Cheng, J. Xiao, Q. Niu, and A. Brataas, Phys. Rev. Lett. **113**, 057601 (2014).
[37] J. Nogués, D. Lederman, T. J. Moran, and I. K. Schuller, Phys. Rev. Lett. **76**, 4624 (1996).
[38] P. Zhang, J. Finley, T. Safi, and L. Liu, Phys. Rev. Lett. **123**, 247206 (2019).
[39] L. Zhu, L. Zhu, and R. A. Buhrman, Phys. Rev. Lett. **126**, 107204 (2021).
[40] I. Gray *et al.*, Phys. Rev. X **9**, 041016 (2019).
[41] K. Garello, I. M. Miron, C. O. Avci, F. Freimuth, Y. Mokrousov, S. Blügel, S. Auffret, O. Boulle, G. Gaudin, and P. Gambardella, Nat. Nanotechnol. **8**, 587 (2013).
[42] J. Kim, J. Sinha, M. Hayashi, M. Yamanouchi, S. Fukami, T. Suzuki, S. Mitani, and H. Ohno, Nat. Mater. **12**, 240 (2013).
[43] C.-F. Pai, Y. Ou, L. H. Vilela-Leão, D. C. Ralph, and R. A. Buhrman, Phys. Rev. B **92**, 064426 (2015).
[44] L. Liu, T. Moriyama, D. C. Ralph, and R. A. Buhrman, Phys. Rev. Lett. **106**, 036601 (2011).
[45] K. Ando, S. Takahashi, K. Harii, K. Sasage, J. Ieda, S. Maekawa, and E. Saitoh, Phys. Rev. Lett. **101**, 036601 (2008).
[46] Y. Wang, P. Deorani, X. Qiu, J. H. Kwon, and H. Yang, Appl. Phys. Lett. **105**, 152412 (2014).
[47] V. Tshitoyan, C. Ciccarelli, A. P. Mihai, M. Ali, A. C. Irvine, T. A. Moore, T. Jungwirth, and A. J. Ferguson, Phys. Rev. B **92**, 214406 (2015).
[48] I. Mihai Miron, G. Gaudin, S. Auffret, B. Rodmacq, A. Schuhl, S. Pizzini, J. Vogel, and P. Gambardella, Nat. Mater. **9**, 230 (2010).
[49] T. Suzuki, S. Fukami, N. Ishiwata, M. Yamanouchi, S. Ikeda, N. Kasai, and H. Ohno, Appl. Phys. Lett. **98**, 142505 (2011).
[50] V. P. Amin and M. D. Stiles, Phys. Rev. B **94**, 104420 (2016).
[51] K.-W. Kim, K.-J. Lee, J. Sinova, H.-W. Lee, and M. D. Stiles, Phys. Rev. B **96**, 104438 (2017).
[52] A. Qaiumzadeh, R. A. Duine, and M. Titov, Phys. Rev. B **92**, 014402 (2015).
[53] H. Nakayama *et al.*, Phys. Rev. Lett. **110**, 206601 (2013).
[54] D. Hou, Z. Qiu, J. Barker, K. Sato, K. Yamamoto, S. Vélez, J. M. Gomez-Perez, L. E. Hueso, F. Casanova, and E. Saitoh, Phys. Rev. Lett. **118**, 147202 (2017).
[55] S. M. Rezende, A. Azevedo, and R. L. Rodríguez-Suárez, J. Appl. Phys. **126**, 151101 (2019).
[56] N. C. Koon, Phys. Rev. Lett. **78**, 4865 (1997).
[57] J. Wu *et al.*, Nat. Phys. **7**, 303 (2011).
[58] M. Finazzi, A. Brambilla, P. Biagioni, J. Graf, G. H. Gweon, A. Scholl, A. Lanzara, and L. Duò, Phys. Rev. Lett. **97**, 097202 (2006).
[59] P. K. Manna and S. M. Yusuf, Phys. Rep. **535**, 61 (2014).
[60] J. Fujii, F. Borgatti, G. Panaccione, M. Hochstrasser, F. Maccherozzi, G. Rossi, and G. van der Laan, Phys. Rev. B **73**, 214444 (2006).
[61] W. Kim, E. Jin, J. Wu, J. Park, E. Arenholz, A. Scholl, C. Hwang, and Z. Q. Qiu, Phys. Rev. B **81**, 174416 (2010).
[62] H. Chen, Q. Niu, and A. H. MacDonald, Phys. Rev. Lett. **112**, 017205 (2014).
[63] S. Nakatsuji, N. Kiyohara, and T. Higo, Nature (London) **527**, 212 (2015).